FUNDAMENTALS & APPLICATIONS

CHEMELECTROCHEM

ANALYSIS & CATALYSIS, BIO & NANO, ENERGY & MORE

Accepted Article

Title: Ultra-fast cycling of nanoscale thin film LiCoO2 electrodes in aqueous electrolytes.

Authors: James Rohan and Tomás M Clancy

To be cited as: *ChemElectroChem* 10.1002/celc.201800822

Link to VoR: http://dx.doi.org/10.1002/celc.201800822

A Journal of

ChemPubSoc Europe

WILEY-VCH

www.chemelectrochem.org

WILEY-VCH

ARTICLE

Ultra-fast cycling of nanoscale thin film $LiCoO_2$ electrodes in aqueous electrolytes.

Tomás M. Clancy,[a] and James F. Rohan*[a]

Abstract: Additive-free nanoscale $LiCoO_2$ thin-films deposited on Si substrates using DC sputtering show exceptional electrochemical performance due to the unique kinetics of the nanoscale thin-film in an aqueous environment. At extremely high scan rates and galvanostatic current densities of up to 100 mV s^{-1} and 200 C respectively, a capacity retention equivalent to 97 mAh g^{-1} (4.8 µAh cm^{-2}, 48.3 µAh cm^{-2} $µm^{-1}$) is obtained. A significant contribution of non-diffusion controlled kinetics in a $LiCoO_2$ electrode is shown.

Introduction

The 'Internet of Things' scenario envisions billions of wireless sensors acting as the environmental interface to provide data that will, amongst other benefits reduce analysis costs, improve safety and predict future trends. Non-rechargeable batteries are the predominant energy source for today's commercial wireless sensors and both the energy and power demands dramatically reduce the lifetime of the primary batteries. The value of the useful data gathered is offset by the frequent battery replacement necessitated by their short lifetimes. The ultimate challenge facing the mass distribution of wireless sensors is meeting the energy and power requirements to match the lifetime of the microdevices[1].

To extend the lifetime, smaller and more energy efficient sensor components and drive electronics are being developed with lower power and energy requirements. Of the available battery technologies Li-ion provides the highest energy density (~270 Wh kg^{-1}) which is essential for miniaturisation and device integration[2]. The limitations of typical organic solvent–based Li-ion batteries include a modest cycle life (<1,000) and low power density (<1,000 W kg^{-1}) which can hamper device operation particularly during the energy intensive periods of sensor measurement and wireless communication. Hybrid systems comprising a significantly smaller energy storage element coupled to an energy harvester are of interest to enable wireless operation over the lifetime of the device[3].

Microbatteries, such as solid-state Li-ion batteries, present a number of potential advantages in the transition from primary to rechargeable batteries for hybrid powered wireless sensors[4]. They have a larger potential energy density due to the removal of inactive binder and conductive additive materials in the cathodes and they offer the potential for Li metal anodes. The solid-state electrolyte significantly improves cycle life (≥ 5,000)[5]. The drawbacks which have limited their use in commercial systems include the need to maintain thin electrodes (at the micron level) particularly for the low electronic conductivity oxide cathodes typically utilised. A cathode with limited thickness and conductivity in combination with a low ionic conductivity solid-state electrolyte results in poor power capabilities and a significant potential drop can occur during high current operation. A small form factor capable of high current operation is critical in the development of next-generation hybrid systems. Dedicated micro power management systems are also required to deal with these issues and that of intermittent energy supply from the harvester which can add further volume and complexity to the system[6].

In a typical thin-film microbattery the faradaic reaction and ion transport are primarily controlled by the solid-state diffusion kinetics in the electrode material. Changing the geometry, size and thickness of the electrodes will have a direct effect on the battery capabilities. Cathodes tend to be the limiting electrode material in batteries due their low electrical conductivity (layered oxide materials) and lower energy density compared to typical anode materials. 3D architectures with a large aspect ratio coupled to nanoscale films are a possible strategy to enable high currents for a hybrid system[7]. In this strategy the energy footprint is primarily dependent on the aspect ratio of the 3D architectures and the power footprint on the thickness of the electrodes. Using the approximation[8] for time (τ) to diffuse in a material of dimension l ($\tau \approx l^2/D$), where D is the diffusion coefficient, it can be estimated that the time taken for Li^+ to diffuse in typical battery materials of micron dimension will be two to three orders of magnitude slower with a corresponding lower power capability than for a nanoscale (≤ 100 nm) material.

Recent research has shown nanoscale film electrodes are not solely diffusion controlled and that pseudo-capacitive intercalation has a significant contribution on the electrochemical performance[9]. Solid-state and organic electrolytes by comparison with aqueous electrolytes tend to have low ionic conductivity and slower diffusion characteristics which have a significant effect on cell performance. The high ionic conductivity and diffusion coefficient of an aqueous electrolyte means that the electrochemical performance is primarily dependent upon the rate of lithiation and delithiation rather than the ion transport in the electrolyte. Analysis of a nanoscale film electrode in an aqueous electrolyte enables the analysis of the electrode performance without the resistive complications of an organic or solid state electrolyte.

The concept of aqueous rechargeable Li-ion batteries was first introduced in 1994 with the use of $LiMn_2O_4$ and VO_2(B) giving a cell potential of 1.5 V for 25 cycles[10]. This smaller potential window limits the suitable electrode materials. One of the most common cathode materials, $LiCoO_2$ (3.9 V vs Li^+/Li) used in organic systems can also be utilised in aqueous systems[11]. As with organic electrolytes side reactions due to the aqueous environment can complicate the lithium intercalation reaction mechanism[12]. As described in a recent review the number of papers published on aqueous lithium battery systems has increased tenfold over a ten year period[13]. While the research

[a] T. M. Clancy, Dr. J.F. Rohan
Electrochemical Materials and Energy
Tyndall National Institute, University College Cork.
Lee Maltings, Cork, Ireland
E-mail: james.rohan@tyndall.ie

into thin-film $LiCoO_2$ has been thorough in organic and solid-state electrolytes, there has been limited analysis for aqueous electrolytes. The majority of analysis on $LiCoO_2$ in an aqueous electrolyte has been directed towards bulky composite electrodes[14]. Such electrodes are porous and contain inactive additives unlike the solid-state thin film materials required for high-power microbatteries.

The nanoscale $LiCoO_2$ thin-films described here were deposited using standard DC sputter processing appropriate for thin film microbattery applications. An aqueous electrolyte is used to investigate the electrochemical properties of a nanoscale $LiCoO_2$ thin-film in order to ensure the performance of the electrochemical cell is solely dependent on the electrode and not influenced by the resistive electrolytes typically used in the investigation of Li-ion electrodes. Cyclic voltammetry and galvanostatic cycling demonstrated charging in less than 18 s, and similarly that the material could be discharged in the same timeframe without altering the characteristic electrochemical profile of $LiCoO_2$.

Results and Discussion

Figure 1a shows the XRD pattern of a typical $LiCoO_2$ thin-film deposited by DC magnetron sputtering. XRD shows crystalline phases of (003) and (104) reflections that have an intensity ratio ($I_{(003)}/I_{(104)}$) of 0.67, indicating that (104) is the dominant phase present and that there is cation mixing within the hexagonal lattice[15]. The (101) and (104) crystalline phases are preferred for $LiCoO_2$ as a lithium battery electrode in which the layered structure is at 10^0 and 35° to the surface, respectively, meaning increased rate capabilities[16]. The (003) crystalline phase on the other hand where the layered structure is at 90° to the surface limits the lithiation/delithiation which can only occur at cracks in the surface[17]. Initially solid-state deposition of $LiCoO_2$ thin-films with a thickness of ≤ 500 nm were (003) dominated with layers ≥ 1 µm preferring (101) and (104) orientations however other factors such as deposition technique, substrate, gas pressure etc. also have a significant influence on crystalline lattice[16a, 18].

$LiCoO_2$ has a space group of $R\bar{3}m$ as verified by the presence of the A_{1g} and E_g peaks in the Raman spectrum of Figure 1b. The E_g peak at 596 cm^{-1} is associated with the stretching of the Co-O bond and the A_{1g} peak at 487 cm^{-1} with the bending of the O-Co-O bonds. The ratio between the intensity of E_g and A_{1g} peaks is ($I_{(Eg)}/I_{(A1g)}$) 0.62, which indicates there is a small amount of c-axis orientation with a random orientation in the film[19]. The vibration of oxygen atoms at the ab and c -axes are related to the E_g and A_{1g} peaks, respectively, and the results are in agreement with the XRD analysis[20]. The full width half maximum (FWHM) of less than 12 cm^{-1} for the A_{1g} peak is a good indication of the thin-film quality[21].

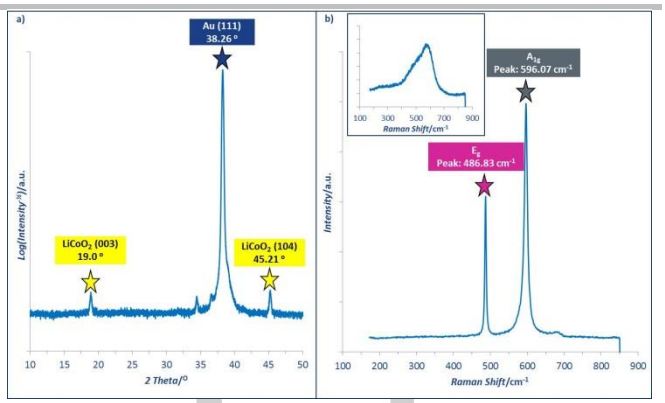

Figure 1. XRD (a) and Raman (b) of rapid thermal annealed (RTA) 100 nm $LiCoO_2$ film. Inset images are of as-deposited 100 nm $LiCoO_2$ film.

A plan view SEM and cross-sectional TEM image for the $LiCoO_2$ deposit is shown in Figure 2. The SEM image indicates large grains without a preferred orientation, while the cross-section shows a rough $LiCoO_2$ surface with an average thickness of 100 nm on 100 nm of Au and 6 nm of Ti in agreement with surface profilometry measurements.

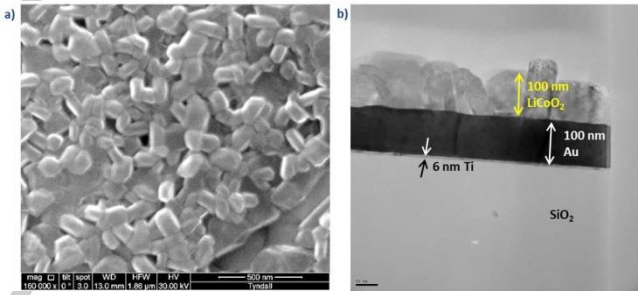

Figure 2. SEM plan view and TEM cross-section of nanoscale-film $LiCoO_2$ on a 100 nm Au current collector that contained a 6 nm Ti base layer to adhere to the 1µm thermal annealed SiO_2 layer on the Si wafer substrate.

The CV analysis in Figure 3 shows a well-defined redox couple for the anodic and cathodic reaction. The peak separations at 1, 20 and 100 mV s^{-1} are 4, 36 and 98 mV, respectively, and are well defined indicating a low overpotential and small electrolyte charge transfer and electrode/electrolyte interfacial resistances. This is in contrast to a composite nanoparticle $LiCoO_2$ electrode that contained an electrically conductive additive in an Li-ion aqueous electrolyte where there is a large increase in overpotential resulting in the distortion of the CV profile with the potential shift of the anodic peak to beyond the extended potential window cut-off value at increasing scan rates[14d, 22]. The thin film (100 nm) cathodes can achieve extremely high currents of up to 10 mA cm^{-2}, appropriate for a wireless sensor during active operation or data transmission. The potential distortion when analysing the characteristics of electrode materials in organic and solid state electrolytes is minimised in the high conductivity aqueous electrolytes.

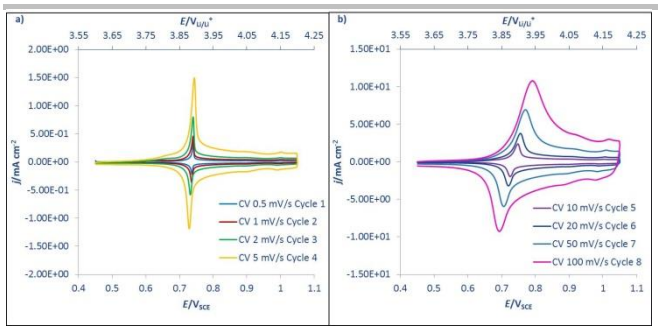

Figure 3. CV of 100 nm $LiCoO_2$ film at 0.5, 1, 2, 5 (a) 10, 20, 50 and 100 mV s^{-1} (b) in 5 M $LiNO_3$ aqueous electrolyte.

The peak current associated with lithium intercalation / deintercalation at layered oxide cathode materials, conventionally a diffusion controlled faradaic reaction within the crystalline structure, is proportional to the square root of the scan rate. Non-diffusion controlled faradaic reactions, dependent on the outer surface area and typically seen in supercapacitor materials, has a linear dependence on the scan rate. The equation for the peak current dependence on scan rate, Eq. 1, is in the form of the power law relationship and can be used to determine the dominating kinetics, Eq. 2.

$$i = av^b \quad (1)$$

$$\log(i) = \log(a) + (b)\log(v) \quad (2)$$

A slope of 0.5 demonstrates diffusion control while a slope of 1 implies non-diffusion controlled lithium storage. In Figure 4a the average slope for cathodic and anodic peaks is 0.69. This means that the lithium storage is dominated by diffusion controlled kinetics but has a significant non-diffusion controlled contribution[23]. This is in strong agreement with the well-defined CV profiles, of Figure 3, at fast scan rates (≥ 20 mV s^{-1}), which suggested that the lithium reaction was not solely diffusion controlled and that the contribution is from a faradaic redox process. Typically non-diffusion controlled contributions in an aqueous systems are from double-layer capacitance (non-faradaic) and/or near surface confined pseudocapacitance (faradaic). As the reaction is clearly faradaic and the lithium ions are intercalated into the $LiCoO_2$ the non-diffusion controlled contribution is intercalation pseudocapacitance[23a]. The contribution of both diffusion and non-diffusion controlled lithium reaction is represented by Eq. 3. That can be rearranged to Eq. 4 so that the $i/v^{0.5}$ is plotted against $v^{0.5}$ with the slope equal to k_1 and the intercept equal to k_2. The contribution of the diffusion and non-diffusion controlled kinetics are quantified using Eqs. 5 and 6, respectively.

$$i = k_1 v + k_2 v^{0.5} \quad (3)$$

$$\frac{i}{v^{0.5}} = k_1 v^{0.5} + k_2 \quad (4)$$

$$\text{Diffusion Controlled} = \frac{k_2 v^{0.5}}{k_1 v + k_2 v^{0.5}} \quad (5)$$

$$\text{Non-Diffusion Controlled} = \frac{k_1 v}{k_1 v + k_2 v^{0.5}} \quad (6)$$

As seen in Figure 4b at slow scan rates, diffusion controlled Li-bulk insertion contribution is the dominant mechanism for energy storage. The contribution of the fast intercalation pseudo-capacitance kinetics is ≤ 20% at scan rates lower than 2 mV s^{-1}. However the intercalation pseudocapacitance kinetics become more dominant at increased scan rates and are responsible for > 50% of the energy storage at scan rates ≥ 50 mV s^{-1} which corresponds to accessing most of the cathode material in under 10 s. The pivotal input of the non-diffusion controlled kinetics, which is considered negligible in commercial Li-ion batteries, allows for lithium energy accessibility at high rate capabilities. This indicates that nanoscale thin-films of $LiCoO_2$ have the ability to achieve high energy and power densities for devices in an appropriate electrolyte.

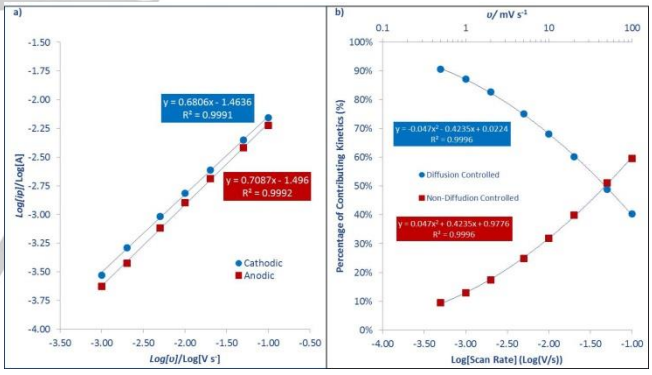

Figure 4. Log[Peak Current] vs. Log[Scan Rate] to determine b-value (a) and percentage of contributing kinetics at various scan rates (b).

The diffusion coefficient was estimated using the Randles-Sevcik equation (Eq. 7).

$$I_p = (2.69 \times 10^5) n^{3/2} A C_{Li} D_{Li}^{1/2} v^{1/2} \quad (7)$$

where I_p is a peak current, n is the number of electrons transferred, A is the active area of the electrode, C_{Li} is the bulk concentration of Li in $LiCoO_2$, D_{Li} is the diffusion coefficient of Li in the thin film electrode, v is the scan rate.

There is a Li concentration gradient across the thin-film electrode during intercalation and for this analysis it is assumed that the

diffusion is one dimensional in the thin-film electrode. This assumption is regularly utilised when determining Li diffusion such as when using electrochemical impedance spectroscopy (EIS), potentiostatic intermittent titration technique (PITT) and galvanostatic intermittent titration technique (GITT)[24]. The diffusion coefficient for lithiation and delithiation was found to be 5.31×10^{-12} and 7.07×10^{-12} $cm^2 s^{-1}$, respectively, which is in line with the literature for thin-film $LiCoO_2$[25].

Galvanostatic cycling was performed at current densities equivalent to C-rates of 3, 5, 10, 20, 50, 100 and 200 C. Figure 5a shows the galvanostatic charge and discharge curves of the fifth cycles in the sequence, while Figure 5b shows the specific capacity of the galvanostatic cycling. The main redox plateau is observed even at 200 C which is agreement with the well-defined peak seen in the CV of Figure 3. Generally the redox plateau decreases and drops in potential at increased C-rates which implies an interference in lithiation/delithiation. The reverse is seen in this study when an increment in C-rate is applied, indicating superior lithiation/delithiation kinetics, in which a well-defined plateau is still present with no drop in potential at a 200 C rate. At a 10 C rate, (full charge/discharge in 6 minutes), a reversible discharge capacity of 108 mAh g^{-1} (5.4 µAh cm^{-2}, 53.9 µAh cm^{-2} $µm^{-1}$), is achieved assuming a film density of 4.98 g cm^{-3} (data sheet density of the sputter target) which is equivalent to 79% of the theoretical capacity (137 mAh g^{-1})[26]. A 20 times increase in current density from 10 C to 200 C, (full charge/discharge in 18 s) exhibit excellent capacity retention with losses of only 12.5% and a capacity of 96.45 mAh g^{-1}. To the best of our knowledge the maintenance of such high capacities for nanoscale $LiCoO_2$ thin-films has not been reported previously[27]. Typically such high C-rates would lead to a significant capacity drop. CV profiles tend to become distorted with peak separation increasing significantly at higher scan rates. Galvanostatic profiles lead to a drop in potential without a significant current plateau and would complicate the use of such a material in a wireless sensor system.

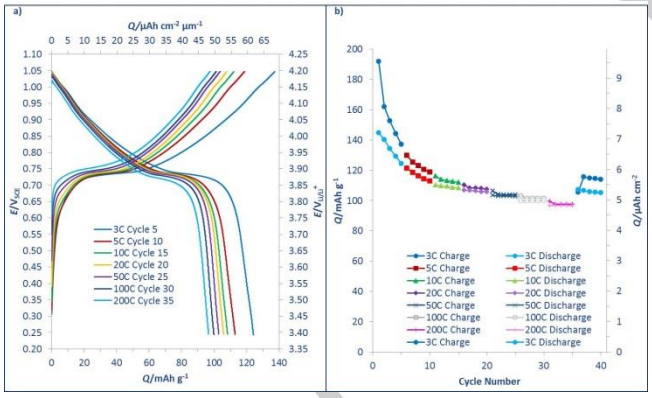

Figure 5. Galvanostatic profiles of a 100 nm $LiCoO_2$ film at various C-rates (a) and summary of galvanostatic cycling capacities (b) in a 5 M $LiNO_3$ aqueous electrolyte.

Longer-term cycling at a 200 C rate was assessed for over 500 cycles is shown in Figure 6. The capacity decreased in the initial cycles (134 cycles) as the system reached equilibrium at which point the capacity value was equivalent to the 200 C value obtained with the $LiCoO_2$ sample used in Figure 5, where the cycling was more intensive. The capacity after 533 cycles was 70 mAh g^{-1} which represents a capacity drop of 0.08 % per cycle over 400 cycles (after stabilisation) as shown in Figure 6. The galvanostatic profiles retain the characteristic plateau during cycling which indicates little interference from side reactions at the electrode / electrolyte interface which are generally seen in organic electrolytes and inhibit the Li^+ ion transport.

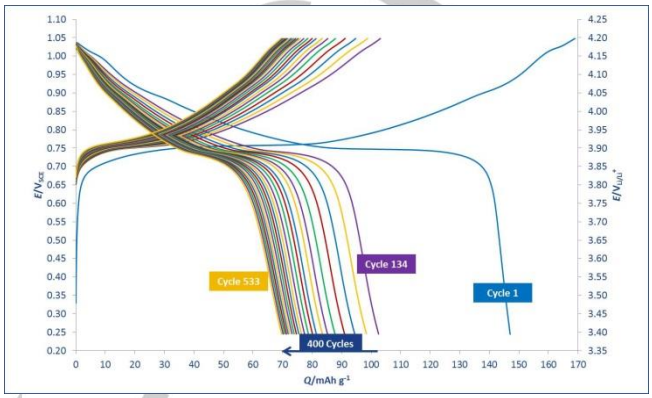

Figure 6. Galvanostatic Cycling of a 100 nm $LiCoO_2$ film at 200 C for 533 cycles in a 5 M $LiNO_3$ aqueous electrolyte.

Conclusions

Nanoscale $LiCoO_2$ films fabricated by DC sputtering show exceptional electrochemical rate capabilities for Li-ion battery applications. At the higher rates intercalation pseudocapacitive storage is dominant and enables the electrochemical kinetics. The charge storage is not limited by the crystalline structure for this nanoscale-film as a result of the decreased diffusion pathway and an increased surface reactivity. The improved wettability of the electrode surface may also play a role in the resultant electrochemical kinetics. At extremely high scan rates and galvanostatic current densities of up to 100 mV s^{-1} and 200 C respectively, a capacity retention equivalent to 97 mAh g^{-1} (4.8 µAh cm^{-2}, 48.3 µAh cm^{-2} $µm^{-1}$) is obtained. Even at only 100 nm thickness the cathodes can achieve desirable high current densities of up to 10 mA cm^{-2}. Nanoscale-film $LiCoO_2$ is a potential electrode for an aqueous electrolyte based battery that can achieve the high current rates during device interrogation for the “Internet of Things” scenario. Aqueous Li-ion batteries can potentially decrease the areal footprint and increase the energy density to more closely match the power requirements of the sensors and electronic micropower management system.

Experimental Section

A stack of Ti (10 nm) and Au (100 nm) was deposited on a 1 µm thermal annealed SiO_2 layer on a 100 mm diameter silicon wafer using metal sputter targets (Kurt J. Lesker) in a DC magnetron (Quorum Q300T D Dual) sputter coating system. The Ti layer acted as an adhesion layer between the SiO_2 substrate and Au current collector. $LiCoO_2$ was deposited, using a $LiCoO_2$ (99.9% purity) sputter target (Kurt J. Lesker) over the Au current collector at a pressure and current of 5×10^{-3} mBar and

150 mA respectively. The $LiCoO_2$ target was cleaned by pre-sputtering for 15 min prior to deposition. All depositions were performed in an Ar environment and deposit thickness monitored using a quartz-crystal monitor system. Deposit thickness was confirmed using a surface profilometer (Tencor alpha-step 200). DC sputtered $LiCoO_2$ is amorphous and is crystallised using rapid thermal annealing (RTA Jipelec 150) at 600^{oC} for 3 min in an Ar environment which has not been investigated previously for aqueous $LiCoO_2$ cathode systems. RTA offers a short operational time and lower energy consumption by comparison with a furnace. The structure and the morphology of the samples were analysed with a scanning electron microscope (FEI Nova 630 Nano-SEM) coupled with an energy dispersive X-ray (EDX) (Hitachi S4000). Transmission electron microscopy (TEM) (was performed using a JEOL 2100 High Resolution TEM), For X-ray diffraction (XRD) a Philips PW3710-MPD with Cu Kα radiation, l = 1.54056 Å, at 45 kV (40 mA) was used and data analysed using Philips X'Pert XRD software). Raman spectroscopy was performed with a Renishaw Invia, 514 nm laser.

Electrochemical measurements were controlled using a CH Instruments 660B potentiostat and a three electrode cell. Cyclic voltammetry (CV) was performed on the $LiCoO_2$ cathode over the potential window of 0.45 to 1.05 V against a saturated calomel electrode (SCE). Galvanostatic cycling was carried out in a potential window of 0.25 to 1.05 V vs SCE at C-rates of 3, 5, 10, 20, 50, 100 and 200 C in which 1 C is equivalent to $LiCoO_2$ being either fully charged or discharged (137 mA g^{-1}) within 1 hour. The electrolyte used was 5 M $LiNO_3$ aqueous solution at a pH of 7 purged with N_2 gas prior to cycling to reduce the amount of dissolved oxygen. A high concentration of $LiNO_3$, neutral pH and little or no dissolved O_2 is critical to remove/suppress the side reactions that are associated with aqueous electrolytes [13]. Delithiated $LiMn_2O_4$ was utilised as the counter electrode. The use of delithiated $LiMn_2O_4$ as a counter electrode rather than a metal counter, (e.g. Pt), is required to achieve stable electrochemical behaviour for extended cycling[13, 14b, 14e, 28]. A metal counter electrode possesses no storage capacity for the Li^+ extracted from the working electrode and would most likely evolve gas as the counter electrode reaction perturbing the electrolyte composition. The delithiated $LiMn_2O_4$ allows for Li^+ to cycle between the electrodes and operates without any significant changes to the chemical or physical properties of the electrolyte. The measurements were carried out under ambient air and at 21^{o}C.

Acknowledgements

The authors would like to acknowledge the financial support from Science Foundation Ireland (SFI) Grant number: 12/IP/1722, Nanomaterials design and fabrication for energy storage and is supported in part by a research grant from SFI co-funded by the European Regional Development Fund under Grant Number 13/RC/2077.

Keywords: $LiCoO_2$ • intercalation pseudocapacitive • cathode • aqueous electrolyte •

[1] D. S. Gardner, C. W. Holzwarth Iii, Y. Liu, S. B. Clendenning, W. Jin, B.-K. Moon, C. Pint, Z. Chen, E. C. Hannah, C. Chen, C. Wang, E. Mäkilä, R. Chen, T. Aldridge, J. L. Gustafson, *Nano Energy* **2016**, *25*, 68-79.

[2] J. Janek, W. G. Zeier, *Nature Energy* **2016**, *1*, 16141.

[3] C. Ó. Mathúna, T. O'Donnell, R. V. Martinez-Catala, J. Rohan, B. O'Flynn, *Talanta* **2008**, *75*, 613-623.

[4] Y. Wang, B. Liu, Q. Li, S. Cartmell, S. Ferrara, Z. D. Deng, J. Xiao, *J. Power Sources* **2015**, *286*, 330-345.

[5] B. J. Neudecker, N. J. Dudney, J. B. Bates, *J. Electrochem. Soc.* **2000**, *147*, 517-523.

[6] W. Wang, J. F. Rohan, N. Wang, M. Hayes, A. Romani, E. Macrelli, M. Dini, M. Filippi, M. Tartagni, D. Flandre, in *Beyond-CMOS Nanodevices 1* (Ed.: F. Balestra), John Wiley & Sons, Inc, **2014**, pp. 249-275.

[7] S. Ferrari, M. Loveridge, S. D. Beattie, M. Jahn, R. J. Dashwood, R. Bhagat, *J. Power Sources* **2015**, *286*, 25-46.

[8] K. M. Abraham, D. M. Pasquariello, E. M. Willstaedt, *J. Electrochem. Soc.* **1998**, *145*, 482-486.

[9] a) M. Zukalová, M. Kalbáč, L. Kavan, I. Exnar, M. Graetzel, *Chem. Mater.* **2005**, *17*, 1248-1255; b) M. Fehse, E. Ventosa, *ChemPlusChem* **2015**, *80*, 785-795; c) C. Rong, S. Chen, J. Han, K. Zhang, D. Wang, X. Mi, X. Wei, *J. Renewable Sustainable Energy* **2015**, *7*, 023104; d) X. Yang, F. Qu, H. Niu, Q. Wang, J. Yan, Z. Fan, *Electrochim. Acta* **2015**, *180*, 287-294; e) K. Naoi, K. Kisu, E. Iwama, S. Nakashima, Y. Sakai, Y. Orikasa, P. Leone, N. Dupre, T. Brousse, P. Rozier, W. Naoi, P. Simon, *Energy Environ. Sci.* **2016**, *9*, 2143-2151; f) M. Fehse, R. Trócoli, E. Ventosa, E. Hernández, A. Sepúlveda, A. Morata, A. Tarancón, *ACS Appl. Mater. Interfaces* **2017**, *9*, 5295-5301.

[10] W. Li, J. R. Dahn, D. S. Wainwright, *Science* **1994**, *264*, 1115-1118.

[11] a) H. Kim, J. Hong, K.-Y. Park, H. Kim, S.-W. Kim, K. Kang, *Chem. Rev.* **2014**, *114*, 11788-11827; b) G. Wang, L. Fu, N. Zhao, L. Yang, Y. Wu, H. Wu, *Angew. Chem. Int. Ed.* **2007**, *46*, 295-297; c) H. Yadegari, A. Jabbari, H. Heli, *J. Solid State Electrochem.* **2012**, *16*, 227-234.

[12] a) H. Manjunatha, G. S. Suresh, T. V. Venkatesha, *J. Solid State Electrochem.* **2011**, *15*, 431-445; b) W. Li, W. R. McKinnon, J. R. Dahn, *J. Electrochem. Soc.* **1994**, *141*, 2310-2316; c) J. Y. Luo, Y. Y. Xia, *Adv. Funct. Mater.* **2007**, *17*, 3877-3884.

[13] N. Alias, A. A. Mohamad, *J. Power Sources* **2015**, *274*, 237-251.

[14] a) G. J. Wang, N. H. Zhao, L. C. Yang, Y. P. Wu, H. Q. Wu, R. Holze, *Electrochim. Acta* **2007**, *52*, 4911-4915; b) R. Ruffo, C. Wessells, R. A. Huggins, Y. Cui, *Electrochem. Commun.* **2009**, *11*, 247-249; c) G. J. Wang, Q. T. Qu, B. Wang, Y. Shi, S. Tian, Y. P. Wu, R. Holze, *Electrochim. Acta* **2009**, *54*, 1199-1203; d) W. Tang, L. L. Liu, S. Tian, L. Li, Y. B. Yue, Y. P. Wu, S. Y. Guan, K. Zhu, *Electrochem. Commun.* **2010**, *12*, 1524-1526; e) R. Ruffo, F. La Mantia, C. Wessells, R. A. Huggins, Y. Cui, *Solid State Ionics* **2011**, *192*, 289-292.

[15] M. Sathiya, A. S. Prakash, K. Ramesha, A. K. Shukla, *Materials* **2009**, *2*, 857-868.

[16] a) J. B. Bates, N. J. Dudney, B. J. Neudecker, F. X. Hart, H. P. Jun, S. A. Hackney, *J. Electrochem. Soc.* **2000**, *147*, 59-70; b) Y. Yoon, C. Park, J. Kim, D. Shin, *J. Power Sources* **2013**, *226*, 186-190.

[17] P. J. Bouwman, B. A. Boukamp, H. J. M. Bouwmeester, P. H. L. Notten, *J. Electrochem. Soc.* **2002**, *149*, A699-A709.

[18] a) L. Bohne, T. Pirk, W. Jaegermann, *ECS Transactions* **2011**, *32*, 17-21; b) H. Y. Park, S. C. Nam, Y. C. Lim, K. G. Choi, K. C. Lee, G. B. Park, H. P. Kim, S. B. Cho, *Korean J. Chem. Eng.* **2006**, *23*, 832-837; c) H. Xia, L. Lu, G. Ceder, *J. Alloys Compd.* **2006**, *417*, 304-310; d) H. Y. Park, S. C. Nam, Y. C. Lim, K. G. Choi, K. C. Lee, G. B. Park, J. B. Kim, H. P. Kim, S. B. Cho, *Electrochim. Acta* **2007**, *52*, 2062-2067; e) K.-T. Jung, G.-B. Cho, K.-W. Kim, T.-H. Nam, H.-M. Jeong, S.-C. Huh, H.-S. Chung, J.-P. Noh, *Thin Solid Films* **2013**, *546*, 414-417; f) J. Xie, N. Imanishi, A. Hirano, M. Matsumura, Y. Takeda, O. Yamamoto, *Solid State Ionics* **2007**, *178*, 1218-1224.

[19] Y. Iriyama, M. Inaba, T. Abe, Z. Ogumi, *J. Power Sources* **2001**, *94*, 175-182.

[20] S.-W. Song, H. Choi, H. Y. Park, G. B. Park, K. C. Lee, H.-J. Lee, *J. Power Sources* **2010**, *195*, 8275-8279.

[21] D. Song, C. Jiang, B.-S. L. Kwak, D. Severin, Electrochemical device fabrication process with low temperature anneal, **2014**, U.S. Patent Application No. 13/951,702, Applied Materials Inc., Google Patents

[22] Q. Liu, M. S. Javed, C. Zhang, Y. Li, C. Hu, C. Zhang, M. Lai, Q. Yang, *Nanoscale* **2017**, *9*, 5509-5516.

[23] a) Y. Wang, Y. Song, Y. Xia, *Chem. Soc. Rev.* **2016**, *45*, 5925-5950; b) K. Brezesinski, J. Wang, J. Haetge, C. Reitz, S. O. Steinmueller, S. H. Tolbert, B. M. Smarsly, B. Dunn, T. Brezesinski, *J. Am. Chem. Soc.* **2010**, *132*, 6982-6990.

[24] a) B. E. Conway, *Electrochim. Acta* **1993**, *38*, 1249-1258; b) M. D. Levi, D. Aurbach, *J. Electroanal. Chem.* **1997**, *421*, 79-88; c) M. D. Levi, D. Aurbach, *Electrochim. Acta* **1999**, *45*, 167-185; d) M. D. Levi, G. Salitra, B. Markovsky, H. Teller, D. Aurbach, U. Heider, L. Heider, *J. Electrochem. Soc.* **1999**, *146*, 1279-1289; e) H. Xia, L. Lu, M. O. Lai, *Electrochim. Acta* **2009**, *54*, 5986-5991.

[25] H. Xia, L. Lu, G. Ceder, *J. Power Sources* **2006**, *159*, 1422-1427.

[26] B. Scrosati, K. Abraham, W. A. van Schalkwijk, J. Hassoun, *Lithium batteries: advanced technologies and applications, Vol. 58*, John Wiley & Sons, **2013**.

[27] Y. Matsuda, N. Kuwata, J. Kawamura, *Solid State Ionics* **2018**, *320*, 38-44.

[28] N. Alias, A. A. Mohamad, *Ceram. Int.* **2014**, *40*, 13089-13096.

Entry for the Table of Contents

ARTICLE

Need for Speed: Li^+ ion transport in nanoscale thin films of $LiCoO_2$ was studied in an environment where rate performance is solely dependent on the electrode. Li^+ intercalation in $LiCoO_2$ is typically diffusion controlled, however, we have shown that non-diffusion controlled pseudo-capacitance intercalation dominates transport kinetics at 100 mV s^{-1} which enables Li^+ transport at high rates in $LiCoO_2$ accessing 71% of the capacity in 6 s (see picture).

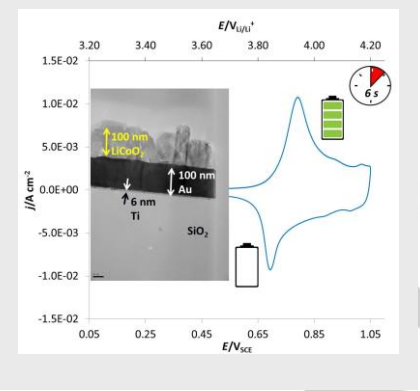

*T. M. Clancy, Dr. J.F. Rohan **

Page No.1 – Page No. 5

Ultra-fast cycling of nanoscale thin film $LiCoO_2$ electrodes in aqueous electrolytes